Published in *The Photogrammetric Record 33 (164): 448-469*

GEOREFERENCED UNDERWATER PHOTOGRAMMETRY TO MAP MARINE HABITATS AND SUBMERGED ARTIFICIAL STRUCTURES

ARNAUD ABADIE[1*], PIERRE BOISSERY[2], CHRISTOPHE VIALA[1]

[1]*Seaviews, La Ciotat, France*

[2]*Agence de l'Eau Rhône-Méditerranée-Corse, Marseille, France*

** Corresponding author: ABADIE@SEAVIEWS.FR*

Abstract

Over the past decade, underwater photogrammetry has been experiencing an increased interest due to the enhancement of camera performance and computing power. This study describes the test of two new methods to perform georeferenced underwater photogrammetry. The first one uses the coupling between photogrammetry by scuba diving and positioning with acoustic data from a multibeam echo sounder; the second one utilises direct positioning technology with a surface floating device (photogrammetric platform). When compared with one another, the platform had a higher mapping efficiency, while being limited by depth and underwater visibility. Georeferenced underwater photogrammetry is expected to have a wide range of applications in the field of marine habitats' conservation such as seagrass meadows and the survey of submerged artificial structures such as artificial reefs and port infrastructure.

KEYWORDS: underwater photogrammetry, georeferencing, marine habitats, mapping, positioning, bathymetry

INTRODUCTION

PHOTOGRAMMETRY ALLOWS THE EXTRACTION of three-dimensional (3D) data by analysing two-dimensional (2D) images, and is commonly divided into three fields of study: terrestrial (close range), aerial and satellite. Aerial photogrammetry has been commonly used over the last two decades to map landscapes with airborne platforms such as unmanned aerial vehicles (UAVs or drones) (Honkavaara et al., 2009). Derived from the techniques developed through terrestrial and aerial methodology, close-range underwater photogrammetry by scuba diving has, over the past few years, become a common tool for mapping marine archaeological sites and creating 3D models of underwater artefacts (Balletti et al., 2015; Drap et al., 2015). Indeed, its early usages date back several decades, as exemplified by Pollio (1968), Hohle (1971) and Leatherdale and Turner (1983). In parallel, innovative devices have been built to map deep ocean resources on a

large spatial scale (Kwasnitschka et al., 2016). Other recent studies have focused on the use of photogrammetry to map and study marine habitats and benthic species such as seagrass meadows (Rende et al., 2015b), sparse coral colonies (Drap et al., 2014) and coral reefs (Burns et al., 2015).

Although underwater photogrammetry benefits from the advances made by terrestrial (close-range) uses, several issues limit their application as a precise mapping tool of the seafloor. The first issue comes from the optical properties of water and more specifically from its refractive index. This characteristic leads to an apparent increase in the focal length of the lens and thus a decrease of the camera's field of view in water compared with land-based photography (Menna et al., 2016). This fact, added to light absorption by water and the resulting reduction of visibility, reduces the portion of the underwater scene photographed and thus the area mapped.

The second issue is also linked with the optical properties of the water and the focal length of the camera lens. It consists of camera lens distortions, primarily radial distortion and chromatic aberration. The former will reduce the geometric accuracy of the imagery and, by extension, affect the shape of the 3D model generated by photogrammetry. This issue has already been tackled in the field of aerial mapping by UAV photogrammetry which may use short focal length lenses (such as fisheye lenses) which have high distortion but cover a wide field of view (Covas et al., 2015). In underwater photogrammetry, calibration techniques must take into account the lens distortion as well as the type of lens port for accurate measurements (Shortis, 2015; Menna et al., 2016). Ports are either of the *flat* or *dome* type. With a flat port objects are magnified, thus apparently increasing the focal length, With dome ports refraction, radial distortion and chromatic aberration are reduced (especially if the dome's radial centre is close to the front node of the lens), thus effectively preserving the focal length of the lens.

The last limitation to the use of underwater photogrammetry as an accurate mapping tool of the seafloor lies in the georeferencing precision. To date, no accurate and transportable underwater positioning system that can be handled without boat assistance exists (Cheng, 2005). A few existing systems rely on acoustic methods and a surface buoy but their deployment is limited due to their cost and limited range (Alcocer et al., 2006; Tan et al., 2010). These technical issues for underwater positioning appear to be a clear limitation for accurate underwater photogrammetric mapping by scuba diving.

Prior to any photogrammetric studies, whether on land or underwater, terminology to describe output quality must be clearly determined. Thus, throughout this work, the term *precision* is used as the repeatability of a result (Granshaw, 2016). *Accuracy* is the closeness of the result of a measurement, calculation or process to an independent, higher-order reference value and is broadly used as an indicator of quality (Remondino et al., 2017). *Spatial resolution* is used as the estimation of the detail perceptible on an image (Granshaw, 2016). Lastly, *georeferencing* refers to fixing photogrammetric output (for example orthophotographs or digital elevation models) to a geodetic framework (Granshaw, 2016).

Taking into account the optical issues linked with water properties and tackling the positioning issue, this work developed two different methods to generate georeferenced underwater maps through photogrammetry. The aims of this study were:

1. Develop and test a method to georeference underwater photogrammetric mapping performed by scuba diving with acoustic data acquired with a multibeam echo sounder (MBES).

2. Develop and test new surface equipment, namely a floating photogrammetric platform incorporating GNSS for georeferenced underwater photogrammetric mapping at shallow depths.
3. Highlight georeferencing and accuracy issues of underwater photogrammetry.
4. Investigate the potential use of these techniques to map and study marine habitats and submerged artificial structures.

The detailed analysis of the precision and accuracy of the two methods developed is not intended in this paper, which rather aims to describe these techniques and investigate their potential applications in underwater photogrammetry for biological studies and bathymetric measures. From this perspective, a qualitative approach was used that relies on the analysis of georeferenced photogrammetric output through the use of new simple metrics.

MATERIAL AND METHODS

Study Area

Study sites were located in La Ciotat Bay(43°10.00561' N; 5°39.11212' E) in the South of France (Fig. 1). Two test sites for each type of method, that is photogrammetry coupled with MBES and the floating photogrammetric platform, making four sites in all, were selected according to the variety of their seafloor characteristics:

1. The P38 wreck (P38) is a Second World War aircraft that crashed in January 1944 and sank to a depth of 38 m.
2. Mugel Creek (MC) is an inlet with shallow rocky beds (from 3 to 14 m in depth) covered by the endemic Mediterranean seagrass *Posidonia oceanica* (L.) Delile.
3. The area mapped in the Marina (M) is located on the outer part of the artificial dike built along a *P. oceanica* meadow.
4. Canonnier Nord (CN) is a shallow rocky bottom with numerous faults and sparse *P. oceanica* meadows.

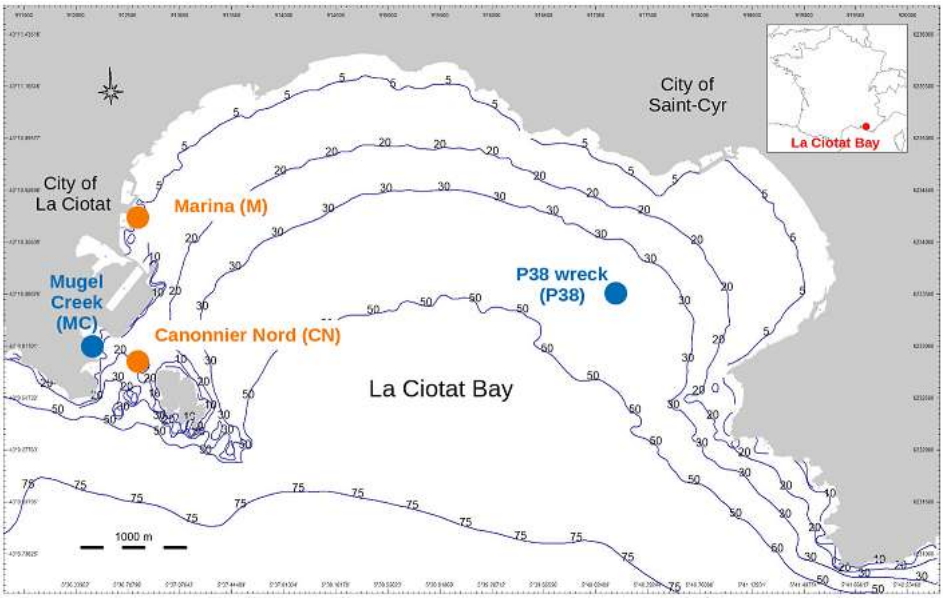

FIG. 1. Study sites within La Ciotat Bay. Blue circles: photogrammetry coupled with multibeam echo sounder. Orange circles: data acquisition with the floating photogrammetric platform. Blue lines: bathymetric contours.

Underwater Photogrammetry Coupled with MBES Data Acquisition

Acoustic sampling on the MC and P38 sites was performed, respectively, in August 2016 and June 2017 with a R2SONIC™ 2022 MBES. Acoustic data were sampled at a frequency of 450 Hz with an individual beam width of 0.9° x 0.9° for a maximum swath sector of 160° with 256 soundings per swath. An inertial navigation system (INS) Applanix I2NS™ was integrated with the MBES and encompassing a full global navigation satellite system (GNSS) mode providing a positioning precision of 1.0 cm along the *X* and *Y* axes and 1.5 cm vertically, a rolling and pitching precision of 0.015° and a precision for heading trajectories of 0.02°. Underwater sound velocity was constantly checked using a Valeport miniSVS sound velocity sensor mounted on the MBES. Additional underwater sound velocity profiles were performed with another miniSVS to detect the possible presence of a thermocline (abrupt temperature gradient) impacting sound propagation. MBES data were processed using the ViewMap software developed by Viala (2015) to obtain a digital elevation model (DEM) for each site. The assessed *XY* accuracy of MBES derived products is 0.78 cm and the minimum *Z* accuracy is 2.8 cm.

Images for photogrammetric reconstruction on site P38 were shot underwater by scuba diving with an 18 megapixel Canon 600D digital single-lens reflex (DSLR) camera in an Ikelite watertight case fitted with a Tokina 10-17 mm fisheye lens with an 8-inch dome port and an Ikelite DS160 external strobe. On the MC site, images were taken with an AEE S70 MagiCam action camera providing photographs with a resolution of 16 megapixel. The stability of cameras inside their housing was tested and found to be good for precise photogrammetric measures; cameras were tightly fixed within housings with a screw to avoid any movement, and the whole system was moved in every direction to check its stiffness. VisualSFM software developed by Wu (2011) was to be used for processing both the P38 and MC sites, but as it may have issues in correcting the inherent radial distortions of fisheye lenses, both cameras in their watertight housing were

pre-calibrated using in-air distortion test targets prior to underwater measurements. A lens profile was then generated using Adobe Lens Profile Creator. Finally, a finer calibration of both cameras was performed using the automated process provided by VisualSFM using a block-invariant solution. VisualSFM uses the scale-invariant feature transform (SIFT) detector to extract points of interest in each photograph. The sparse reconstruction of the point-of-interest cloud was then run using the sparse reconstruction process , followed by a dense reconstruction using Yasutaka Furukawa's PMVS/CMVS (Patch- and Clustering- Multi-view Stereo; Furukawa and Ponce, 2010) used in VisualSFM. An N-View Match (NVM) file containing point cloud's information (point coordinates and camera positions) was finally obtained.

In order to georeference the point cloud generated by photogrammetry, NVM files were exported to the ViewMap software (Viala, 2015) where they were combined with DEMs from the MBES data to create a photogrammetric DEM. This process, based on a simplex algorithm, also known as a similarity, 3D conformal or seven-parameter transformation, as described by Press et al. (1996), takes place in two steps:

1. Both models were manually oriented by successive scaling, rotations and translations in three dimensions to provide a best fit and optimising the simplex algorithm calculation.
2. The simplex algorithm calculation was then run. The simplex method developed by Dantzig et al. (1955) relies on the minimisation of constraints through the optimization of a cost function which corresponds to the mean of the altitude differences between the two models. In this case, the usual seven variables were considered: *X*, *Y*, *Z* offsets (translations), scaling and three rotations. The simplex algorithm is executed using constraints which force computing around the results of the first manual solution to avoid divergences toward false solutions due to a high number of local minima.

Direct Positioning with the Floating Photogrammetric Platform

In order to compare the efficiency of both photogrammetric methods to generate DEMs with the one of MBES techniques, acoustic data on M and CN sites were sampled in August 2017 and September 2016, respectively. Photogrammetric data on M and CN sites were collected in August 2017 and September 2017, respectively, using a floating photogrammetric platform developed in the framework of this study. This new surface device consisted of a camera protected by a waterproof case mounted on the underside of a floating system on a stiff aluminium support and linked with a real-time kinematic (RTK) GNSS placed on the upper side on a PVC , together wirh a GNSS antenna (Fig. 2(b)). The camera is a mirrorless Sony A6000 in an Ikelite housing fitted with a Sony 10-180 mm OSS lens protected by a 6" dome port. Since the camera was not mounted with a fisheye lens, the whole system, i.e. camera and lens in the watertight case, was calibrated using the automated calibration provided by VisualSFM using a block invariant solution. The RTK GNSS was a North GNSS RTKite Module Receiver integrated on the floating platform (Fig. 2(a)) and providing real-time positioning with about centimetre accuracy (8 mm horizontally and 15 mm vertically). The camera and GNSS system were linked with a transistor-transistor logic (TTL) cable, modified from underwater photography equipment, to trigger positioning when a photo was shot.

The platform is light (about 10 kg) and compact (115 cm x 70 cm). It can be handled by a single person on the surface who swims slowly to allow a high overlap between

photographs and avoid blurring from camera shake. Photographs are taken using a time-lapse mode at a rate of one picture per second, each image being georeferenced through the GNSS synchronisation. Vertical and horizontal offsets between the GNSS antenna reference point (ARP) and the camera sensor were measured directly on the whole system through repetitive measurements with a rigid ruler. These offset values were incorporated into the data treatment and analysis process.

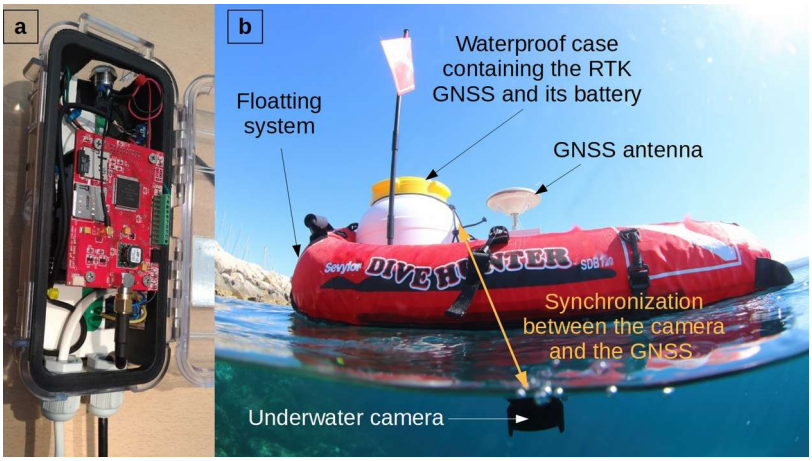

Fig. 2. (a) North RTK GNSS modified for synchronisation with the camera. (b) The underwater photogrammetric platform producing georeferenced photographs. Photographs: Arnaud Abadie.

Raw positioning data from the RTK GNSS were treated in ViewMap to match with the photos using time synchronisation. “Real” camera trajectories were then computed from offsets. Photographs were treated in VisualSFM through the same process as for images shot by scuba diving, with the difference that the pairwise matching option was activated using the location data to generate a pair list and optimise calculation time. The NVM file was finally exported to the ViewMap software where a DEM was built by computing the point-cloud characteristics and corrected positioning data.

XYZ Accuracy and Spatial Resolution Estimation

The two photogrammetric DEMs generated with the floating platform were compared with MBES-based models. It should be noted that MBES models in this work were considered as references for comparison with photogrammetric results, due to the proven accuracy of the acoustic equipment employed. The root square mean (RMS) discrepancy between the photogrammetric and MBES models was computed for *X*, *Y* and *Z* in ViewMap according to the following equation:

$$\sigma_X^2 = \frac{\sum_{i=1}^{n_X} \Delta X_i^2}{n_X}; \sigma_Y^2 = \frac{\sum_{i=1}^{n_Y} \Delta Y_i^2}{n_Y}; \sigma_Z^2 = \frac{\sum_{i=1}^{n_Z} \Delta Z_i^2}{n_Z} \quad (1)$$

where X^2_X, Y^2_Y and Z^2_z, represent the variances of the *X*, *Y* and *Z* coordinates, ΔX, ΔY and ΔZ are coordinate differences, and n_X, n_X and n_Z are the number of differences. Maps

synthesising the RMS error on both sites were generated using the ViewMap software. This estimation required direct GNSS data, so only results provided by the floating platform could be analysed.

The ground sampling distance (GSD) for the floating platform (the distance between the centre of two pixels on the ground) was calculated as follows:

$$GSD = \frac{S_w * H * 100}{F_R * imW} \quad (2)$$

where S_W is the sensor width of the camera in millimetres, H the distance between the sensor and the seafloor in metres, f_R the real focal length of the camera in millimetres (taking into account the capture size and the water's optical properties) and imW is the image width in pixels.

2D and 3D Reconstruction

Two types of representation were obtained for each site from computation of the georeferenced DEM and the photogrammetric data, namely camera position and orientation for each image. 2D representation was in the form of a mosaic of georeferenced underwater orthophotographs; a 3D model (mesh) was textured with the pictures.

Orthophotographs with a pixel resolution of 2 mm (including DEM information) were generated using a specific function of the ViewMap software. The orthophotographs' high resolution proved to exceed standard image formats (such as .png or .jpg) and had to be exported in tile matrix set (TMS) format. Thus, a software extension was developed in the framework of this study to produce georeferenced photographs with zoom properties based on the tile system (Fig. 3). Through their computation, tiles provide an optimal resolution at each zoom level without superfluous calculation. A set of photographs was chosen in ViewMap to allow the texturing process using mesh software whilst avoiding the intensive calculation requirements for large numbers of photographs. NVM files containing the photogrammetric characteristics of the selected photographs for mesh texturing were finally produced with ViewMap for 3D reconstruction.

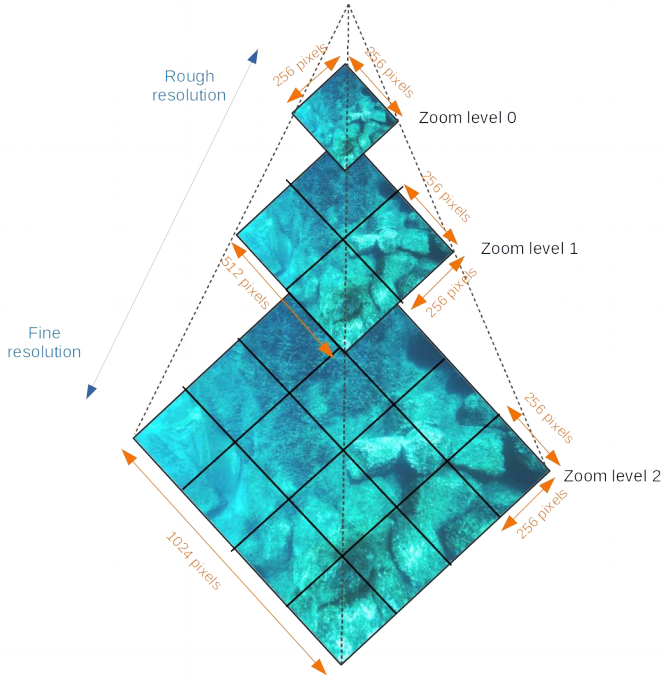

FIG. 3. Illustration of the tile system used for underwater orthophotographs mosaics.

Analysis of Photogrammetric Techniques and Features of 3D Models

Four simple quantitative metrics were calculated to investigate the functioning of the two photogrammetric methods and highlight the complexity of 3D models. The first two metrics concern the photograph requirement and the sampling efficiency. The photo density (PD), meaning the number of photographs per square metre, was calculated for each site as follows:

$$PD=PN_{DEM}/TA \quad (3)$$

where PN_{DEM} is the total number of photographs used for DEM reconstruction and TA the total area mapped (in m^2). PD is expressed in photos.m^{-2} and highlights the sampling effort required according to the area mapped. A high PD indicates an important sampling effort for a relatively small area. The second metric, the mapping efficiency (ME), corresponds to the area mapped per time unit:

$$ME=TA/AD \quad (4)$$

where AD is the acquisition duration in minutes. ME is expressed in $m^2.min^{-1}$: the higher is its value, the more efficient is the mapping process.

The other two metrics investigate the 3D models' complexity and the texture quality. The face density (FD) provides information on the complexity of the 3D structure by computing the number of faces forming the mesh and the area mapped:

$$FD=FN/TA \quad (5)$$

where FN is the face number. FD is expressed in faces.m-2. Complex 3D reconstruction has a high FD while simple 2D meshing has a lower FD.

The last metric describes the texture quality (TQ) by computing the density of faces per photograph:

$$TQ=FN/PN_{text} \quad (6)$$

where PN_{text} is the total number of photographs used to texture the mesh. TQ is expressed in faces.photo^{-1}. A low TQ indicates a higher photographic resolution per face and thus a finer texture of the whole model.

RESULTS

The area mapped ranged from 111 m² (P38) to 4080 m² (CN) and the number of photographs from 790 to 4800 (Table I). The photo density showed differences between the sites sampled by scuba diving (7.1 and 5.8 photos.m^{-2} for P38 and MC respectively) and those mapped with the floating photogrammetric platform (1.8 and 0.9 photos.m^{-2} for M and CN respectively). Similarly, the mapping efficiency was higher on photogrammetric acquisitions made with the floating platform (10.7 and 17.0 m^{-2} min^{-1} for M and CN respectively) than for those performed by scuba diving (1.2 and 6.9 m^{-2}.min^{-1} for P38 and MC respectively). *XYZ* accuracy was of several decimetres (0.48 m and 0.51 m for M and CN sites respectively). The two maps of DEM comparison between photogrammetry and MBES showed that most of the negative *X*, *Y*, *Z* errors where found at low depths where the seascape was uneven. Positive errors were the highest at the greatest depths and on areas covered by seagrass meadows (Fig. 6).

TABLE I. Characteristics of the photogrammetric acquisition on the four study sites.

P38: P38 wreck. MC: Mugel Creek. M: Marina. CN: Canonnier Nord.

Site	*Data Acquisition*	*Min. depth (m)*	*Max. depth (m)*	*Area mapped (m²)*	*Number of images*	*Image density (photo. m^{-2})*	*Duration (min)*	*Mapping efficiency (m^2.min^{-1})*	*Orthophotograph resolution (cm)*	*XYZ accuracy (m)*
P38	Scuba diving	37.0	38.5	111	790	7.1	90	1.2	0.10	-
MC	Scuba diving	4.1	14.3	823	4800	5.8	120	6.9	0.36	-
M	Platform	1.6	7.6	1284	2360	1.8	120	10.7	0.28	0.48
CN	Platform	4.3	18.6	4080	3746	0.9	240	17.0	0.28	0.51

A finer DEM was obtained by photogrammetry than by MBES on the P38 site (Figs. 4(a)

and 4(b)). On the MC site as well, the DEM's resolution was higher by photogrammetry than MBES (Figs. 4(c) and 4(d)). On the sites sampled with the floating photogrammetric platform, a finer DEM was produced by photogrammetry on the M site (Figs. 5(b) and 5(b)). DEMs on the CN site appeared similar with some disparities at the shallowest depths (Fig. 5(c) and 5(d)). Disparities between the depth measured were observed between DEMs generated by MBES and those computed by photogrammetry (Figs. 4 and 5).

Although the orthophoto mosaic of the P38 wreck showed high distortions due to the complex three-dimensional characteristics of the submerged aircraft and their projection onto a 2D representation (Fig. 8(a)), details of the wreck structure were clearly visible (for example wheels, engines, helix). The orthophotographs' resolution of Mugel Creek allowed the identification of the *P. oceanica* meadow on rocky beds (Fig. 8(b)) as well as the detection of several sessile species (for example the algae *Asparagopsis armata* Harvey and the starfish *Echinaster sepositus* Retzius). Similarly, *P. oceanica* meadow was observed on the rocky seafloor of the Canonnier Nord's mosaic (Fig. 8(d)). Smaller species were also identified such as the algae *Codium bursa* (Olivi) Agardh. On the Marina site, an extensive *P. oceanica* meadow with sand patches was clearly recognisable (Fig. 8(c)). Wreck parts as well as miscellaneous waste and discarded objects (such as. tyres) were identified within the sand patches.

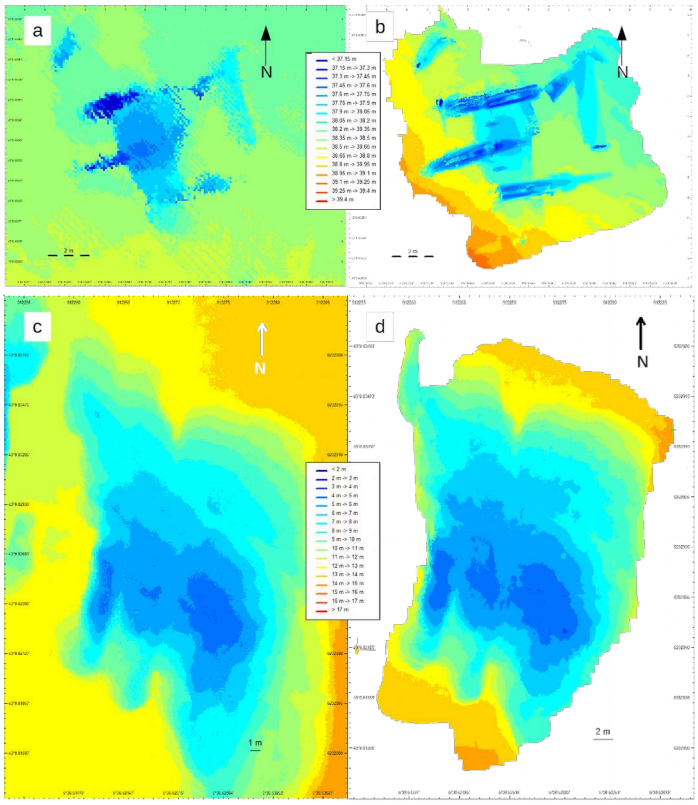

FIG. 4. Digital elevation models (DEMs) georeferenced with a multibeam echo sounder (MBES). (a) P38's DEM by MBES; (b) P38's DEM from photogrammetry by scuba diving; (c) Mugel Creek DEM by MBES; (d) Mugel Creek DEM from photogrammetry by scuba diving.

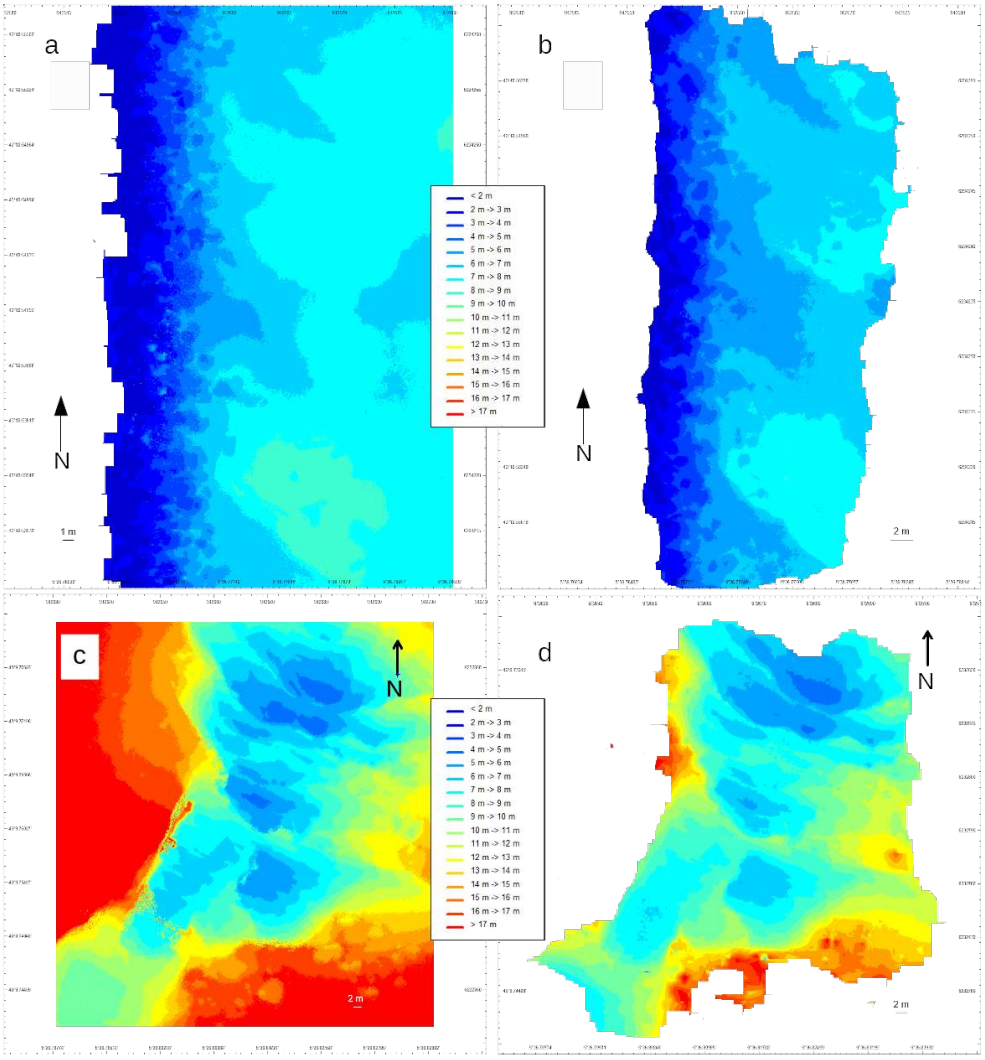

FIG. 5. Digital elevation models (DEMs) georeferenced with a multibeam echo sounder (MBES) or the floating photogrammetric platform. (a) Marina DEM by MBES; (b) Marina DEM by the photogrammetric platform; (c) Canonnier Nord DEM by MBES; (d) Canonnier Nord DEM by the photogrammetric platform.

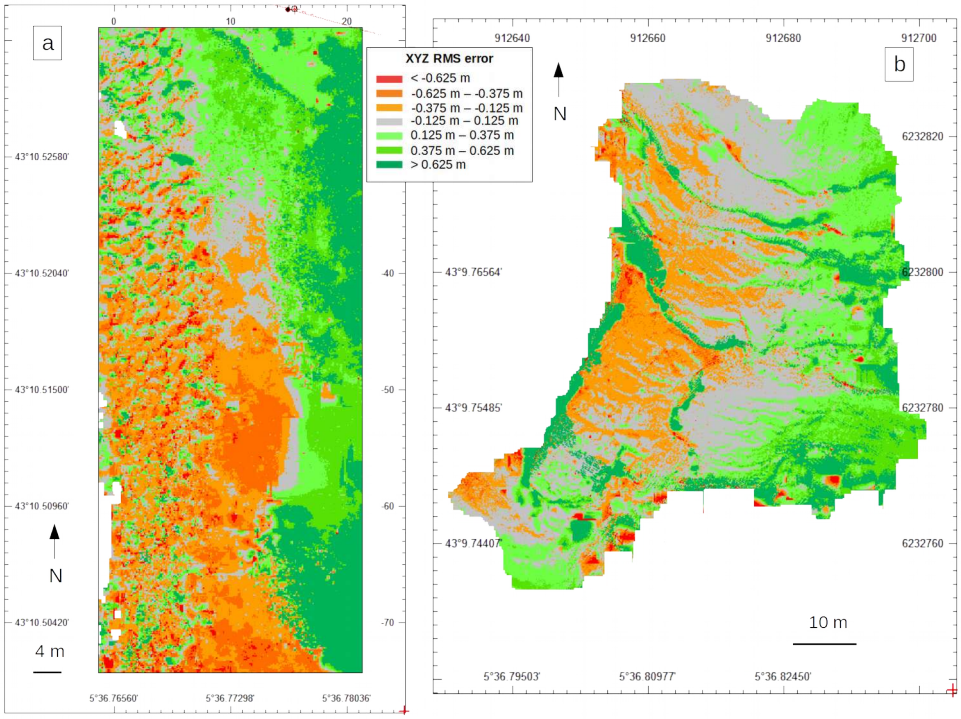

FIG. 6. Map of negative (red to orange) and positive (shades of green) *X*, *Y*, *Z* RMS errors from comparison of photogrammetric and MBES DEMs. (a) Marina; (b) Canonnier Nord.

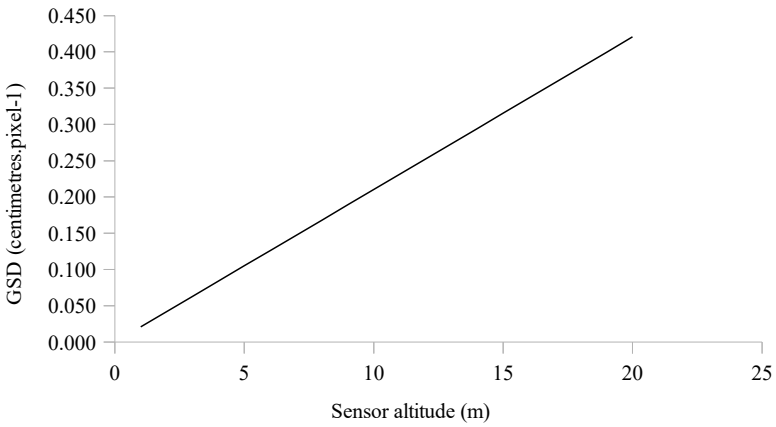

FIG. 7. Ground sampling distance (GSD) in centimetres given the sensor altitude of the floating platform.

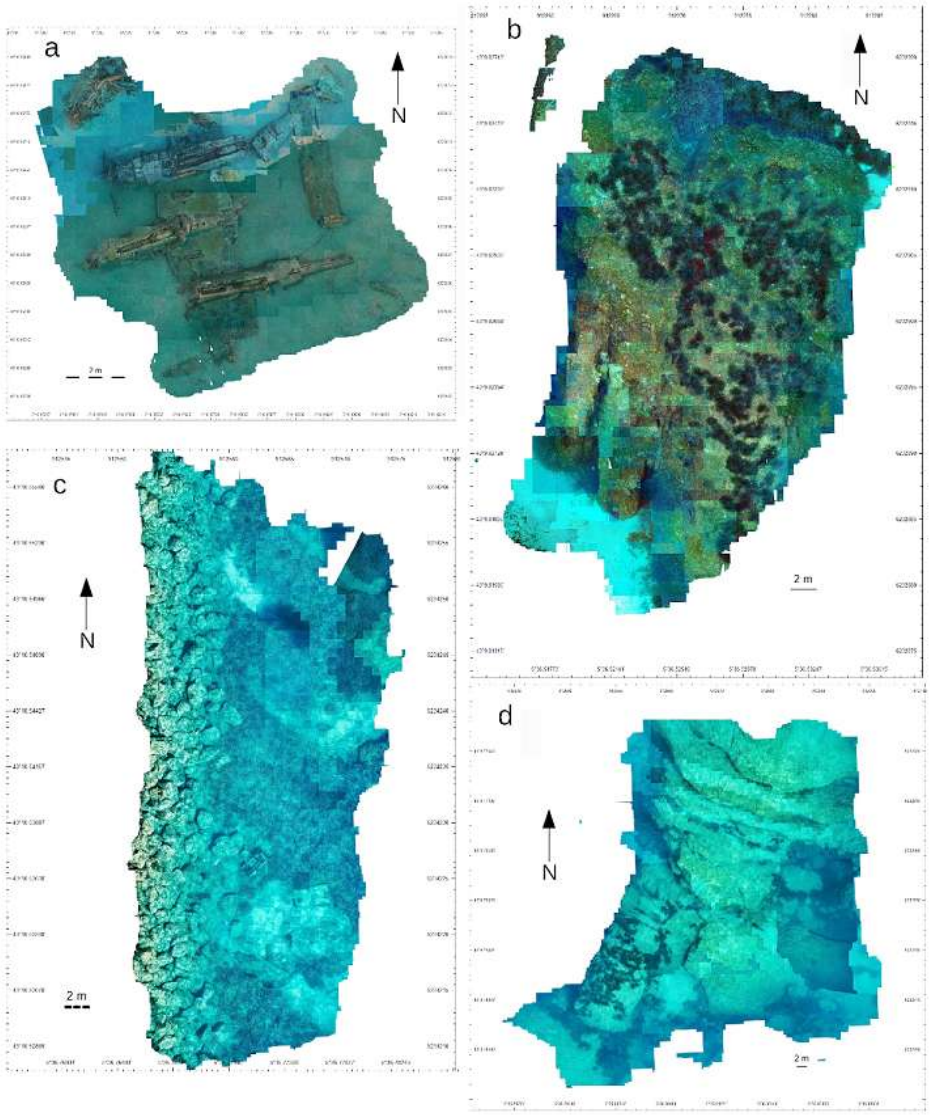

FIG. 8. Orthophoto mosaics generated by photogrammetry. (a) P38 wreck; (b) Mugel Creek; (c) Marina; (d) Canonnier Nord.

All the meshes created during this study can be freely viewed online (in low resolution to ease web navigation) at the https://sketchfab.com/seaviews. Textured 3D models showed the highest image details on the P38 site (Fig. 9) with a texture quality (TQ) of 2998 faces per photo while the structure complexity of the aircraft was the highest among the four sites studied with a face density (FD) of 16 477 faces.m^{-2} (Table II). The MC and CN sites had a similar TQ of 22 752 and 24 578 faces.photo^{-1} respectively, while the complexity of CN site was higher than MC with 7 665 faces.m^{-2} versus 1 539 faces.m^{-2} (Table II).

TABLE II. Mesh characteristics for each site and their quality and complexity metrics. P38: P38 wreck. MC: Mugel Creek. M: Marina. CN: Canonnier Nord.

Site	*P38*	*MC*	*M*	*CN*
Number of vertices	961 452	1 740 290	1 375 875	1 295 119
Number of faces	1 828 978	3 253 545	2 585 202	2 433 226
Area mapped (m^2)	111	823	1 284	4 080
Vertix density ($vertices.m^{-2}$)	8 662	2 115	1 072	317
Face density ($faces.m^{-2}$)	16 477	1 539	2 413	7 665
No. of texture photos	610	143	60	99
Texture quality ($faces.photo^{-1}$)	2 998	22 752	43 087	24 578

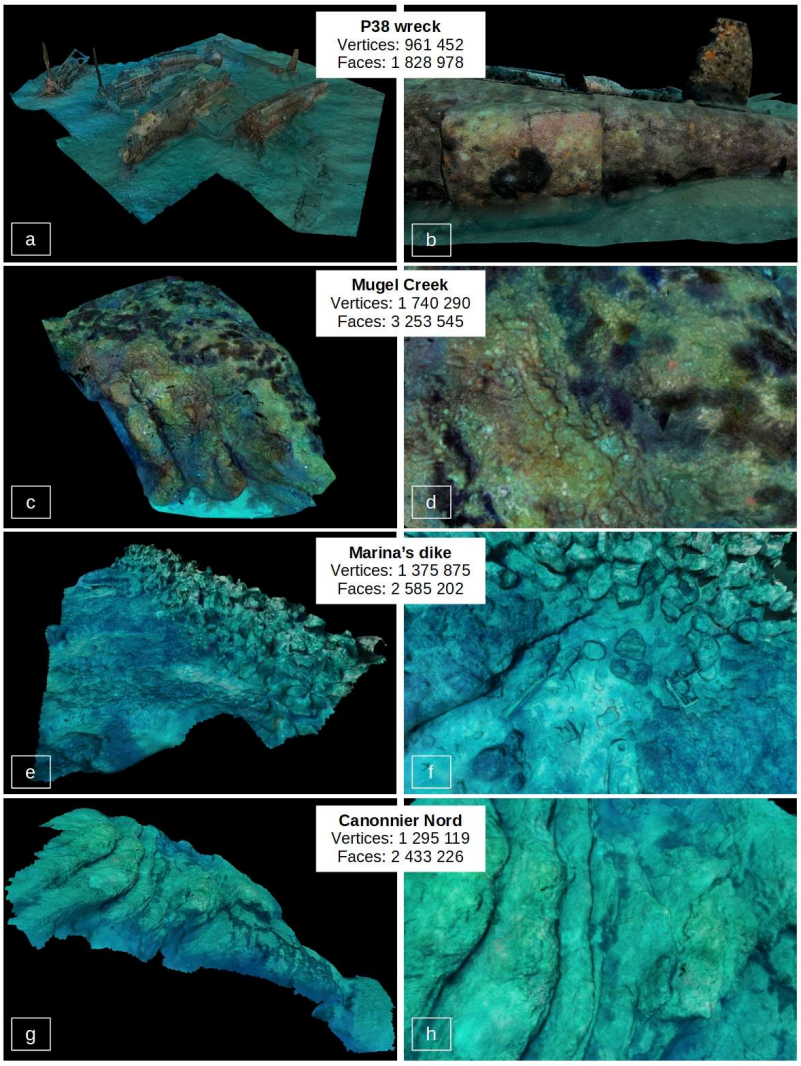

FIG. 9. Perspective and detailed views of the textured 3D models generated by underwater photogrammetry with their numbers of vertices and faces at: (a) and (b) P38 wreck; (c) and (d) Mugel Creek; (e) and (f) Marina; (g) and (h) Canonnier Nord.

DISCUSSION

This research investigated the potential of two methods (scuba diving with an MBES and a floating photogrammetric platform incorporating GNSS) to georeference various products from underwater photogrammetry such as DEMs, orthophotographs and photo-textured 3D models. Given the results of this first study, the authors were able to determine advantages and limitations of the two approaches as well as identifying potential applications for marine habitat mapping and monitoring.

Advantages and Limitations of the Two Methods

Both methods proved their capacity to provide georeferenced output through photogrammetry. However, many disparities concerning their efficiency were highlighted by these initial tests. The first difference, which is quite obvious, lies in the maximum depth at which each technique can be applied (Table III). Although photogrammetry by scuba diving was performed at a maximum depth of 38 m in this study, it can also be performed by deeper divers, autonomous underwater vehicles (AUVs) (Kwasnitschka et al., 2016) and remotely operated vehicles (ROVs), while remaining in the depth range of a MBES for positioning. The same cannot be said for the floating platform, which is limited by underwater visibility as it is operated at the water surface. The maximum depth at which photogrammetric measurements were performed was 16 m with good weather conditions. The maximum depth to generate usable pictures appears to be around 10 m in the Mediterranean Sea (Fig. 10). This is mainly due to the light absorption by the water column thus leading to issues for human interpretation and computer-based image analysis (Bryson et al., 2016).

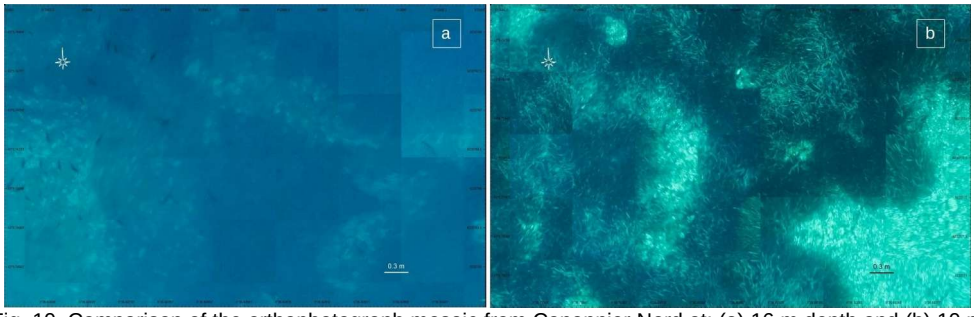

Fig. 10. Comparison of the orthophotograph mosaic from Canonnier Nord at: (a) 16 m depth and (b) 10 m depth.

What the floating platform lacks in depth range it gains on many other aspects of the data acquisition and treatment, in particular at the level of the operability. The platform required just a single swimmer and operated by snorkelling, while a team of divers is compulsory to take the pictures by scuba diving. The better operability of the floating platform over photogrammetry by scuba diving leads to its higher mapping efficiency and thus a reduction of the image density required to map an area (Table II). In summary, for the same acquisition time, areas about two times wider are mapped with the floating platform.

By allowing a direct positioning of each photograph taken, the platform provides a more precise geolocation of all photogrammetric output. This characteristic also greatly reduces

the photograph treatment required in VisualSFM by facilitating the use of the pairwise matching option. The use of such an option results in a linear increase of processing time when the number of pictures increases, instead of an exponential one in the case of photographs shot by scuba diving without positioning data.

The final advantage of the floating platform over photogrammetry by scuba diving is its cost effectiveness. Considering that a scuba diving team, as well as a boat equipped with recent MBES technologies operated by technician specialised in underwater acoustics, are required to obtain georeferenced output from photogrammetry, it appears safe to say that the use of the platform is more cost effective (Table III).

TABLE III. Advantages (+) and limitations (-) of the two techniques of underwater photogrammetry.

	MBES geolocation and scuba diving	*Photogrammetric floating platform*
Depth range	++	-
Operability	+	+++
Mapping efficiency	+	++
Area mapped	-	++
Positioning precision	+	++
Data processing efficiency	-	++
Cost effectiveness	--	++

Positioning Accuracy and Resolution of Photogrammetric Products

Although previous work on underwater photogrammetry uses various positioning systems and methods to georeference output from their underwater data, the evaluation of positioning accuracy by underwater photogrammetry remains scarce at best. Depending on the purpose of the study, photogrammetric outputs are frequently not referenced at all (Eric et al., 2013; Raoult et al., 2016), are merely scaled (Drap et al., 2014; Figueira et al., 2015) or are referenced only in a local system (Burns et al., 2015). Georeferenced underwater photogrammetry is rarer. It may be performed by unmanned vehicles such as AUVs through their navigation system (Kwasnitschka et al., 2016), or by underwater remotely operated vehicles (ROVs) with acoustic transducers (Drap et al., 2008) and towed devices (Rende et al., 2015a). Although producing high-resolution orthophotographs and 3D models, these techniques have a low positioning accuracy, of the order of several metres, due to the distance between the AUV/ROV and the main ship providing geolocation for the first two (Paull et al., 2014); and the uncertainties generated by the length and angle of the cable towing the device for the latter (El-Hawary, 2000). Finally, a direct positioning method was performed by Balletti et al. (2015) using a GNSS antenna mounted on a rope to position salient points at very shallow depths (under 3 m). This technique is an easy way to georeference photogrammetric output but is strongly limited by depth and is only suitable for small areas (about 200 m²).

When compared with all these georeferencing methods, the use of the photogrammetric platform with mastered offsets, repetitive settings, a direct location with the GNSS synchronisation and a “hull” camera fixed directly under the GNSS antenna, produces the most accurate (decimetre) photogrammetric output in positioning. In many ways, the platform adopts the conceptual model and the direct georeferencing method of unmanned aerial vehicles (UAVs) which has already proved its capacity in providing accurate positioning (Mostafa and Hutton, 2001; Grayson et al., 2018).

One of the main factors degrading the positioning accuracy lies in the distortions of the camera lenses used. Distortions induced by wide-angle lenses and the dome ports, which mandatory for underwater data acquisition, are thus one of the main drawback of photogrammetry in general (Shortis, 2015). The present study chose to use the automated calibration provided by VisualSFM which provides the most optimal solution after trying additional software to correct lens distortions, such as Photoshop and RawTherapee. Obviously optical distortions, even when corrected through calibration, lead to positioning issues. This phenomenon has been studied in aerial photogrammetry by several authors including Yastikli and Jacobsen (2005) who found a root mean square difference between 6.6 and 7.1 cm in the *X* direction and between 8.6 and 28.5 cm in *Z* (height), depending on the rigour of the calibration method. Underwater, it is hard to assess in what proportion of the distortions affecting positioning accuracy are due to the optical properties of the water itself; these are not always predictable and may change during the photogrammetric capture of images (for example water layers with heterogeneous temperatures and particle charging).

Although this issue has not been documented yet, the authors can provide some precautions that must be taken prior to data acquisition and processing to reduce underwater positioning uncertainty. First, all the lever-arm offsets between the positioning device and the camera must be identified and precisely measured. Secondly, a cautious air, rather than underwater, calibration of the optical devices used must be performed (Lavest et al., 2003; Shortis, 2015). Then, during the data acquisition phase, the smooth running of the positioning system must be regularly checked. It is also mandatory to consider the sea level at the time of the acquisition when using a floating device, even in areas with low tides such as Mediterranean Sea. Finally, positioning data should be used, if possible, prior to the 3D reconstruction process to improve the accuracy of camera positions.

When comparing DEMs (or bathymetric equivalents) obtained from photogrammetry with those obtained from MBES, a wide range of variation (up to a couple of metres in extreme cases) was observed in the vertical (*Z*) direction. Since bathymetry using MBES has a proven capacity to provide very accurate underwater DEMs with a georeferencing precision of a few centimetres in the *X*, *Y* and *Z* directions, it seems logical that the range of measured variation of up to several decimetres reflects the low *Z* accuracy of underwater DEMs derived from photogrammetry. These differences can be explained by a combination of *XY* systematic errors, an inadequate calibration of the camera and the optical properties of the water environment. Moreover, major positive *X*, *Y*, *Z* RMS errors were observed on the canopy of the seagrass meadows, which is continuously shifting, as well as on complex 3D underwater structures such as the blocks comprising the dike and faults of rocky substrates. To the authors’ knowledge, no previous study has confronted the bathymetric output of those two techniques and further investigations are required to produce accurate underwater DEMs comparable to those generated with acoustic techniques.

When looking at the GSD, it can be seen that the results were always under 0.4 cm, even when approaching the extreme range of the floating platform (Fig. 7). The spatial resolution of the underwater photogrammetry performed from the surface was therefore far higher than that from aerial photogrammetry, which is of several centimetres (Colomina and Molina, 2014). This pattern was mainly due to the sea level (floating) nature of the platform and the water's optical properties. The spatial resolution of photographic products derived from underwater photogrammetry from the surface is thus high enough to perform advanced picture analysis.

Potential Applications to Surveying Marine Habitats and Artificial Underwater Structures

Georeferenced underwater photogrammetry allows marine surveys to be conducted in various fields of science. As mentioned earlier, its main current use concerns submerged archaeological sites (Drap et al., 2008). However, it may be used for other purposes and more specifically in the field of seascape studies (Rende et al., 2015a) and the survey of artificial underwater structures.

A wide range of data on marine habitats and species is expected to be extracted from the output of georeferenced underwater photogrammetry. 3D models seem particularly relevant to study the complex 3D structure of seagrass seascapes (Abadie et al., 2018; Rende et al., 2015b) and coral reefs (Figueira et al., 2015). Orthophotographs appear as the most interesting type of output. Their potential for millimetre pixel resolution allows the identification of sessile benthic species such as algae and echinoderms. Moreover, they have proved to be an accurate data source to map the limits of marine habitats by providing information equivalent to ground-truth photographs (Bryson et al., 2017). The coupling of orthophotographs with 3D models is also expected to be an accurate method to assess and survey mechanical impacts such as anchoring damage to seagrass meadows. In the framework of seagrass seascape studies, the two positioning methods in this paper, namely using a floating platform or an MBES, are complementary, depending of the depth investigated.

Submerged artificial structures are another potential subject of study through georeferenced photogrammetry. It has already been proven to be a useful tool to model shipwrecks (Eric et al., 2013; Menna et al., 2013). Given the high resolution of photo-textured 3D models, it seems conceivable to monitor the colonisation processes of marine life on ship and aircraft wrecks through photogrammetry. This use, however, does not require georeferenced data since scaling alone is sufficient to identify and measure the fixed fauna and flora. Georeferenced underwater photogrammetry is expected to be more useful to survey the physical evolution of submerged structures such as dikes, artificial reefs and fragile wrecks.

CONCLUSION

Georeferenced underwater photogrammetry is possible through various techniques and is accurate enough to provide valuable data on marine habitats and artificial submerged structures. However, it will not, in the near future, replace other underwater mapping methods. Currently only acoustic sensors, such as side-scan sonar and MBES, are able

to provide extensive and accurate maps of the seafloor. Compared with such acoustic techniques, photogrammetry requires very significant computing power to generate high-resolution models for areas extending to several hundreds of square kilometres. Due to this limitation together with other issues such as reliable colour reproduction, it is currently only practicable to map small marine areas photogrammetrically. There is also a strong need for an improvement in the georeferencing accuracy of photogrammetric output from underwater scenes for the operational use of bathymetric data.

Maybe the true interest of underwater photogrammetry lies in aspects other than extensive maps of the seafloor. First of all, photogrammetry is currently the only technique that provides a sub-centimetric resolution for underwater mapping. This key characteristic is particularly appreciated in underwater archaeology and for the monitoring of deep technological infrastructure. It has also great potential for photo-realistic referenced data providing non-destructive ways of studying marine diversity and habitats. Additionally, the 3D models produced may enhance public awareness of the impact of human activities on marine ecosystems. Since it is predicted that underwater positioning accuracy will increase within the next decade, it is now time to apply underwater photogrammetry to conservation and start to consider how to couple it with classical monitoring techniques.

ACKNOWLEDGEMENTS

This research was funded by: (i) the Banque Publique d'Investissement France in the framework of the French Tech grant; (ii) the French Ministry of the Environment (Ministère de la Transition Ecologique et Solidaire) in the framework of the GreenTech Verte grant; and (iii) by the French Water Agency (Agence de l'Eau Rhône-Méditerranée-Corse).

REFERENCES

ABADIE, A., PACE, M., GOBERT, S. and BORG, J. A., 2018. Seascape ecology in *Posidonia oceanica* seagrass meadows: linking structure and ecological processes for management. *Ecological Indicators*, 87: 1-13

ALCOCER, A., OLIVEIRA, P. and PASCOAL, A., 2006. Underwater acoustic positioning systems based on buoys with GPS. *Eighth European Conference on Underwater Acoustics*, Carvoeiro, Portugal. 8 pages.

BALLETTI, C., BELTRAME, C., COSTA, E., GUERRA, F. and VERNIER, P., 2015. Underwater photogrammetry and 3D reconstruction of marble cargos shipwreck. *International Archives of Photogrammetry, Remote Sensing and Spatial Information Sciences,* 40(5): 7-13.

BRYSON, M., FERRARI, R., FIGUEIRA, W., PIZARRO, O., MADIN, J., WILLIAMS, S., BYRNE, M., 2017. Characterization of measurement errors using structure-from-motion and photogrammetry to measure marine habitat structural complexity. *Ecology and Evolution*, 7(15): 5669–5681.

BRYSON, M., JOHNSON-ROBERSON, M., PIZARRO, O., WILLIAMS, S.B., 2016. True color correction of autonomous underwater vehicle imagery. *Journal of Field Robotics*, 33(6): 853–874.

BURNS, J. H. R., DELPARTE, D., GATES, R. D. and TAKABAYASHI, M., 2015. Integrating structure-from-motion photogrammetry with geospatial software as a novel technique for quantifying 3D ecological characteristics of coral reefs. *PeerJ,* 3: e1077. DOI: 10.7717/peerj.1077. 19 pages.

CHENG, W.-H., 2005. Study mobile underwater positioning system with expendable and multi-functional bathythermographs. *Ocean Engineering*, 32(3): 499–512.

COLOMINA, I., MOLINA, P., 2014. Unmanned aerial systems for photogrammetry and remote sensing: a review. *ISPRS Journal of. Photogrammetry and Remote Sensing*, 92: 79–97.

COVAS, J., FERREIRA, V. and MATEUS, L., 2015. 3D reconstruction with fisheye images: strategies to survey complex heritage buildings. *Digital Heritage 2015*, Granada, Spain. Pages 123–126. DOI: 10.1109/DigitalHeritage.2015.7413850.

DANTZIG, G., ORDEN, A. and WOLFE, P., 1955. The generalized simplex method for minimizing a linear form under linear inequality restraints. *Pacific Journal of Mathematics*, 5(2):183–195.

DRAP, P., MERAD, D., HIJAZI, B., GAOUA, L., NAWAF, M. M., SACCONE, M., CHEMISKY, B., SEINTURIER, J., SOURISSEAU, J.-C. and GAMBIN, T., 2015. Underwater photogrammetry and object modeling: a case study of Xlendi wreck in Malta. *Sensors*, 15(12): 30351–30384.

DRAP, P., MERAD, D., MAHIDDINE, A., SEINTURIER, J., GERENTON, P., PELOSO, D., BOÏ, J.-M., BIANCHIMANI, O. and GARRABOU, J., 2014. In situ underwater measurements of red coral: non-intrusive approach based on coded targets and photogrammetry. *International Journal of Heritage in the Digital Era*, 3(1): 123–139.

DRAP, P., SEINTURIER, J., CONTE, G., CAITI, A., SCARADOZZI, D., ZANOLI, S. M. and GAMBOGI, P., 2008. Underwater cartography for archaeology in the VENUS project. *Geomatica*, 62(4): 419–427.

EL-HAWARY, F., 2000. *The Ocean Engineering Handbook*. CRC Press, Boca Raton, Florida, USA. 416 pages.

ERIC, M., BERGINC, G., PUGELJ, M., STOPINSˇEK, Z. and SOLINA, F., 2013. The impact of the latest 3D technologies on the documentation of underwater heritage sites. *Digital Heritage International Congress 2013*, Marseille, France. Pages 281–288.

FIGUEIRA, W., FERRARI, R., WEATHERBY, E., PORTER, A., HAWES, S. and BYRNE, M., 2015. Accuracy and precision of habitat structural complexity metrics derived from underwater photogrammetry. *Remote Sensing*, 7(12): 16883–16900.

FURUKAWA, Y. and PONCE, J., 2010. Accurate, dense, and robust multiview stereopsis. *IEEE Transactions on Pattern Analysis and Machine Intelligence*, 32(8): 1362–1376.

GRANSHAW, S. I., 2016. Photogrammetric terminology: third edition. *Photogrammetric Record*, 31(154): 210–252.

GRAYSON, B., PENNA, N. T., MILLS, J. P. and GRANT, D. A., 2018. GPS precise point positioning for UAV photogrammetry. Photogrammetric Record, 33(164): xxx-xxx

HOHLE, J., 1971. Reconstruction of underwater object. *Photogrammetric Engineering*, 37(9): 948-954.

HONKAVAARA, E., ARBIOL, R., MARKELIN, L., MARTINEZ, L., CRAMER, M., BOVET, S., CHANDELIER, L., ILVES, R., KLONUS, S. and MARSHAL, P., 2009. Digital airborne photogrammetry – a new tool for quantitative remote sensing? A state-of-the-art review on radiometric aspects of digital photogrammetric images. *Remote Sensing*, 1(3): 577–605.

KWASNITSCHKA, T., KÖSER, K., STICKLUS, J., ROTHENBECK, M., WEISS, T., WENZLAFF, E., SCHOENING, T., TRIEBE, L., STEINFÜHRER, A. and DEVEY, C., 2016. DeepSurveyCam—a deep ocean optical mapping system. *Sensors*, 16(2): 164.

LAVEST, J.-M., RIVES, G. and LAPRESTÉ, J.-T., 2003. Dry camera calibration for underwater applications. *Machine Vision and Applications*, 13(5): 245–253.

LEATHERDALE, J. D. and TURNER, D. J., 1983. Underwater photogrammetry in the North Sea. *Photogrammetric Record*, 11(62): 151–167.

MENNA, F., NOCERINO, E., FASSI, F. and REMONDINO, F., 2016. Geometric and optic characterization of a hemispherical dome port for underwater photogrammetry. *Sensors*, 16(1): 48. 21 pages.

MENNA, F., NOCERINO, E., TROISI, S. and REMONDINO, F., 2013. A photogrammetric approach to survey floating and semi-submerged objects. *SPIE*, 8791: 87910H. 15 pages.

MOSTAFA, M. M. R. and HUTTON, J., 2001. Direct positioning and orientation systems. How do they work? What is the attainable accuracy. *American Society of Photogrammetry and Remote Sensing Annual Meeting*, St. Louis, Missouri, USA. Pages 23–27.

PAULL, L., SAEEDI, S., SETO, M. and LI, H., 2014. AUV navigation and localization: a review. *IEEE Journal of Oceanic Engineering*, 39(1): 131–149.

POLLIO, J., 1968. *Applications of Underwater Photogrammetry*. Naval Oceanographic Office (NSTL Station MS), Washington DC, USA. 38 pages.

PRESS, W. H., TEUKOLSKY, S. A., VETTERLING, W. T. and FLANNERY, B. P., 1996. *Numerical Recipes*. Cambridge

University Press, Cambridge, UK. 949 pages.

RAOULT, V., DAVID, P. A., DUPONT, S. F., MATHEWSON, C. P., O'NEILL, S. J., POWELL, N. N. and WILLIAMSON, J. E., 2016. GoPros™ as an underwater photogrammetry tool for citizen science. *PeerJ*, 4: e1960. DOI: 10.7717/peerj.1960.

REMONDINO, F., NOCERINO, E., TOSCHI, I., MENNA, F., 2017. A critical review of automated photogrammetric processing of large datasets. *International Archives of Photogrammetry, Remote Sensing and Spatial Information Sciences*, 42: 591–599.

RENDE, F. S., IRVING, A. D., BACCI, T., PARLAGRECO, L., BRUNO, F., DE FILIPPO, F., MONTEFALCONE, M., PENNA, M., TRABUCCO, B. and DI MENTO, R., 2015a. Advances in micro-cartography: a two-dimensional photo mosaicing technique for seagrass monitoring. *Estuarine, Coastal and Shelf Science*, 167: 475–486.

RENDE, F. S., IRVING, A. D., LAGUDI, A., BRUNO, F., SCALISE, S., CAPPA, P., MONTEFALCONE, M., BACCI, T., PENNA, M. and TRABUCCO, B., 2015b. Pilot application of 3D underwater imaging techniques for mapping *Posidonia oceanica* (L.) delile meadows. *International Archives of Photogrammetry, Remote Sensing and Spatial Information Sciences*, 40(5): 177-181.

SHORTIS, M., 2015. Calibration techniques for accurate measurements by underwater camera systems. *Sensors*, 15(12): 30810–30826.

TAN, H.-P., GABOR, A. F., EU, Z. A. and SEAH, W. K. G., 2010. A wide coverage positioning system (WPS) for underwater localization. *IEEE International Conference on Communications*, Cape Town, South Africa. 5 pages.

VIALA, C., 2015. ViewMap https://seaviews.fr/en/services-3/software-development [Accessed 9th October 2018]

WU, C., 2011. *VisualSFM: A Visual Structure from Motion System*. http://ccwu.me/vsfm/doc.html [Accessed 3rd October 2018]

YASTIKLI, N. and JACOBSEN, K., 2005. Influence of system calibration on direct sensor orientation. *Photogrammetric Engineering & Remote Sensing*, 71(5): 629–633.

Résumé

Au cours de la dernière décennie, la photogrammétrie sous-marine a suscité un intérêt grandissant grâce à l'amélioration des performances des appareils photo et de la puissance des ordinateurs. Ce travail décrit le test de deux nouvelles méthodes de photogrammétrie sous-marine géoréférencée. La première utilise le couplage entre la photogrammétrie réalisée en plongée sous-marine et le positionnement avec des données acoustiques d'un sondeur multifaisceaux ; la seconde utilise une technique de positionnement direct avec un dispositif de surface (plate-forme photogrammétrique). La comparaison entre ces deux techniques montre que la plate-forme offre une meilleure précision de positionnement, limitée toutefois par la profondeur et la visibilité. La photogrammétrie sous-marine géoréférencée possède un vaste potentiel d'applications dans les domaines de la conservation des habitats marins comme les herbiers, et de la surveillance des structures artificielles submergées comme les récifs artificiels et les infrastructures portuaires.